Fuel Processing Technology 263 (2024) 108119

Contents lists available at ScienceDirect

Fuel Processing Technology

journal homepage: www.elsevier.com/locate/fuproc

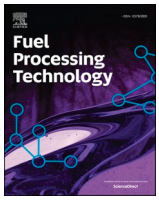

Crystal structure of asphaltene under mechanical stress of ball milling

Fahad Al-Ajmi, Jun Li *

Department of Chemical & Process Engineering, University of Strathclyde, James Weir Building, 75 Montrose Street, Glasgow G1 1XJ, UK

ARTICLE INFO

Keywords:
Asphaltene
Crystallite parameters
Mechanical stress
Ball Milling
XRD analysis

ABSTRACT

This work aims to investigate the structural behaviour of asphaltene under mechanical stress using ball milling. Asphaltene samples were collected and separated from Kuwait export crude using n-heptane and subsequently ball milled for up to 24 h. X-ray diffraction was used to provide an insight into asphaltene macrostructure properties, which subsequently utilised to determine crystallite parameters. The results showed that the mechanical stress has a great influence on these structural parameters, with an increase of the aromatic sheet's inter-layer distance from 3.6 Å to 3.9 Å. While the height of stacked aromatic sheets per cluster and the number of stacked aromatic sheets per cluster decreased from 24.6 Å to 9.3 Å and 8 to 3.2, respectively. A significant increment in the aromaticity value was also observed after the ball milling experimentations, indicating mechanical stress induces cyclisation and aromatisation. The XRD profiles of the higher milling time samples reveals a high background intensity. This suggests a formation and/or increasing the proportion of highly disordered materials. In addition, the effects magnitude on asphaltene crystal parameters between the mechanical stress against heat stress was compared. The results showed core structural parameters are more sensitive to mechanical stress over heat stress.

1. Introduction

A major focus of the recent United Nations Conference on Climate Change (COP28) was implementing the Paris Agreement, including transitioning from inefficient fossil fuels to renewable energy to achieve zero-net target by 2030 [1]. Apparently, oil industry is confronted with challenges that could destabilize the economy as well as impede the zero-net progress, especially heavy crude oils are believed to significantly contribute to the carbon dioxide emissions [2,3]. This is due to the presence of more complex fractions in the heavy oil phase, in particular asphaltenes [4–7].

Petroleum asphaltene has been gaining a lot of interest as a source of fuel and carbon-based materials over the last decade's [8–10]. Asphaltene is the heaviest molecular weight petroleum fraction and is known as the most complex and polarized structural compound in the crude oil phase. Unlike other common hydrocarbons, asphaltene is defined based on its solubility rather than chemical structure [11]. It consists of a mixture of diverse hydrocarbons of unknown molecular structures farmed as aggregated clusters [12]. It is widely accepted that the molecular architecture of asphaltene constitutes of a cyclic island of aromatics core linked by saturated chains including aliphatic carbons of different lengths and condensed naphthenic rings [13]. In addition, within the asphaltene matrix, heteroatoms (S, N, O) and trace elements (Ni, V, Fe) are distributed heterogeneously in different forms of functional groups and organometallic complexes [14–16]. The contents of those compounds vary greatly depending on the oil's origin [17,18,]. However, efficient processing of asphaltene remains a technical challenge. With this regard, the nature of asphaltene molecular properties is required to be further understood.

To aid the measurement of changes on asphaltene molecules during refining and upgrading processing, a set of mathematical equations were proposed to calculate its crystal parameters [12,19]. A range of analytical techniques, such as Raman spectroscopy, C-NMR and X-ray diffraction (XRD), can be implemented to derive the crystallite parameters, and thus its molecular structure is determined [20]. These parameters include the layer distance between the neighbouring aromatic sheets (d_m), distance between the saturated fragments (d_γ), aromatic sheets average diameter (L_a), average height of stacked aromatic sheets per cluster (L_c), and the number of stacked aromatic sheets per cluster (M) [21–23].

The practices of ulterining asphaltene molecular structure have been mostly focused on the thermal treatment [24–27]. However, behaviour of the thermally treated asphaltene samples' parameters related to the aromatic core geometry (i.e., M) follows almost the same pattern [28–31]. For instance, Hauser et al. pyrolysed atmospheric residue

* Corresponding author.
E-mail addresses: fahad.alajmi@strath.ac.uk (F. Al-Ajmi), jun.li@strath.ac.uk (J. Li).

https://doi.org/10.1016/j.fuproc.2024.108119
Received 22 May 2024; Received in revised form 10 August 2024; Accepted 18 August 2024
Available online 27 August 2024

Nomenclature

KEC	Kuwait Export Crude
BM	Ball Milling
γ-band	Spacing between aliphatic layers
002-band	Spacing between core aromatic layers
d_m	Layer distance between the neighbouring aromatic sheets
d_y	Distance between neighbouring aliphatic chains including saturated rings
L_a	Average diameter of the core aromatic sheets
L_c	Height of stacked aromatic sheets per cluster
NO_{ar}	Average number of aromatic rings per sheets
M	Number of aromatic sheets per stacked cluster
C_{au}	Number of carbon atoms in the aromatic unit
f_a	Aromaticity index of asphaltene molecules
AR	Atmospheric residue
VR	Vacuum residue
x	Heteroatoms as single atom or in their associated functional group

asphaltene at 412 °C for 7-h roughly, it was reported that the M value changed from 6 to 7 [32]. Whereas the reported value of the parent sample was 8 [33], indicating heat treatment has a slightly effect on stacked aromatic sheets per cluster. As the consequence, the structural behaviour of asphaltene molecules has been primarily investigated as a function of various ranges of heat stress [31].

Alternatively, mechanical stress can be used to achieve unique properties by manipulating molecular structures [34]. Ball milling (BM) is globally recognised as a mechanical tool with superior ability to refine coarse materials into delicate powders of finer particle size, accomplished by rotating cylindrical vessels charged with hundreds of rigid balls of free movement [35]. During milling process, the collusion between balls generates a continues sheer stress, that would alter energy level in molecular structure [36]. As milling times increase, mechanical stress results in lattice defects caused by severe plastic deformation. This promotes the transformation and/or destabilisation of the crystal phase for a wide variety of chemical elements [36,37]. After BM, the crystallite parameters of substance are affected to a significant extend [38]. Essentially, BM can be controlled by adjusting milling parameters (i.e., speed, time, etc) to offer different form of forces such as friction, collusion and sheer, the combination of these forces able to induce molecular structure changes by modifying crystal parameters [39].

Few studies utilised BM technology on various petroleum-related substances. For instance, Chen et al [40], found that combining ball milling with ozone-catalyst is an effective process for oily sludge treatment from the tank bottom. It was found that the oil content in dry oily sludge decreased from 33.9 to 10.2%. They also noticed that the content of asphaltene decreased from 12.30 to 2.94 wt% using only BM. Welham et al [41], examined the reaction kinetic of ball milled Collie coal over various BM times. They found that the onset combustion temperature and the pyrolysis behaviour of longer milled sample greatly overcome the shorter milled samples. Other study implemented BM to enrich the low-grade high sulfur petcoke with high nitrogen content, urea was used (mixed) as nitrogen precursor. It was reported that after 24 h milling time, the petcoke' elemental property improved with an increment in the nitrogen content from 1.40 to 7.00 wt% [42]. In contrast, a short BM of Athabasca asphaltene was conducted to evaluate the property of the formed soot during pyrolysis at different particle sizes. Despite of particles surface modification, it was found the short milling time (1-h) has negligible effect [43]. Indicating that relying only on morphological changes might not be adequate.

All these previous studies have mainly relied on observing the morphological property (i.e., surface modification such as porosity and particle size) of petroleum related substance including asphaltene to demonstrate the influence of the mechanical stress. However, asphaltene is highly complicated substance of complex organic molecules. Thus, gaining insights into the molecular structure of asphaltene allows estimating several important aspects such as molecules geometry, crystal property and phase transformation as well as its refractory nature as function of various molecular arrangement. Therefore, an investigation of asphaltene's crystal parameters under mechanical stress using ball milling is highly required.

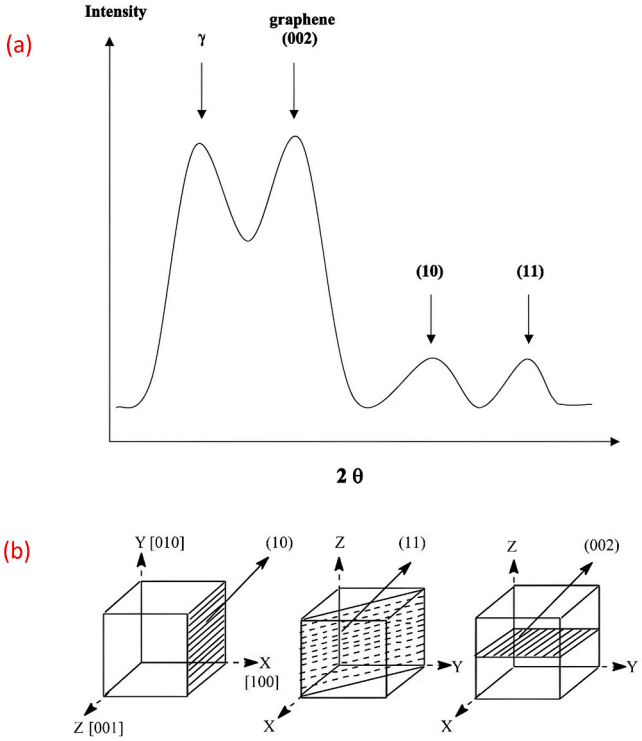

Fig. 1. The position of the four diffracted asphaltene bands (a) and planes (b) [45].

Molecular parameters of asphaltene are critical in understanding its structural behaviour under different reaction environment. XRD measurements has been often utilised to provide macro-structure property of asphaltenes based on computing the dimensions of the unit cell [31,44]. It is known that the XRD patterns of crude oil asphaltene consists of four major peaks appear over the 2θ region at around 20°, 25°, 40° and 80°: the first two peaks related to γ-band and graphene (002)-band, corresponding to the distance between the saturated chains and space between the stacked aromatic sheets respectively [19], and the last two peaks come from the in-plane aromatics structure, which are identified as 10-band and 11-band,corresponding to the average size of aromatic sheet [17,45], as shown in Fig. 1.

This work will determine a full set of crystallite parameters of KEC asphaltene after BM using XRD. The structural behaviour as a function of different milling times will be analysed and discussed for the first time in comparison to thermally treated asphaltene samples. Revealing asphaltene structural behaviour under diverse stresses should help refineries and downstream sectors developing optimal processing for heavy and extra-heavy crude oil. Moreover, the findings of this work will demonstrate the effects magnitude between mechanical and thermal stress on asphaltene structural parameters. This also should provide insights into effective methods of asphaltene valorisation.

Table 1
General properties of KEC asphaltene.

Proximate analysis %			Ultimate analysis %						KEC Composition %	
Volatile	Fixed carbon	Ash	C	H	N	S	O	H/C	Asphaltene	Maltenes
53	43.7	3.3	80.29	7.54	0.81	9.89	1.47	1.13	2.75	97.24

2. Methodology

2.1. Asphaltene sampling and processing

2.1.1. Asphaltene sampling

Asphaltene samples were separated and collected from Kuwait Export Crude (KEC) oil based on the IP 143/90 (ASTM D6560) standard [46]. With a ratio of 30 mL liquid n-heptane to each 1 g of KEC crude oil, 1.5 L of pre-heated n-heptane solution at 67 °C was mixed with 50 g of KEC sample. The mixture was stirred for 2 h then left over night to allow the sedimentation of solid asphaltenes particles at the bottom of the formed solution. A filtration system using Whatman paper (8 μm Whatman) was constructed to separate asphaltene from the solution. Asphaltene particles were deposited on the paper surface, whereas the maltenes are collected at the bottom of flask.

The filter paper was then washed using Soxhlet method to remove any remaining maltenes from the collected asphaltenes. Liquid n-heptane was used for one day till the maltenes were completely removed, followed by liquid toluene to separate the asphaltene from the filter paper. Eventually, the collected toluene- asphaltene solution was placed inside oven that operated at around 100 °C and left for about one day inside the fume hood till complete evaporation of toluene. The resultant asphaltene was collected in form of aggregated black-shinny particles using lab stainless steel micro spatula. Around 1.35 g of asphaltene was recovered for each 50 g of KEC crude oil sample. Table 1 shows the general elemental property of the KEC asphaltene sample.

2.1.2. Ball milling of asphaltene samples

Around 5 g of the KEC asphaltene sample was charged into the 220 mL stainless steel hardened vial together with 50 tool-steel balls (4 g each ball with 10 mm in diameter), at 40:1 ball-powder weight ratio. The system was sealed under atmospheric conditions, then was mounted on high energy planetary ball mill (Retsch PM 400, Germany). The BM process was carried out at room temperature for 30 min, 1 h, 3 h, 6 h, 12 h and 24 h of milling times at 300 RPM. At each run, the vial was unsealed inside a fume hood to collect about 50 mg of the milled sample.

2.1.3. XRD tests of KEC asphaltene

XRD analysis of each KEC asphaltene sample was conducted to quantify the impact of ball milling on its crystallite parameters. The apparatus (Rigaku-SmartLab, Japan) was operated with CuKα (λ =1.5405 Å) using 9 kW Intelligent X-ray diffraction, the scanned patterns of 2θ range was selected in-between 5° to 90° at 0.05 step size with 2 min-1 s/step. After obtaining the diffracted patterns of each sample, the baseline was corrected and subsequently deconvoluted into Lorentzian curves to extract the characteristic peaks information including the area, intensity and positions, as well as the full width at half maximum and interplanar distance [47]. To ensure that the derived crystallite parameters are as accurate as possible, both the baseline and profile fitting were corrected and measured three times to achieve a high coefficient of determination ($R^2 \approx 0.99$).

2.2. XRD data processing

Molecular architecture provides an insight into the structural change of crude oil asphaltene during upgrading process. In x-ray diffraction, the positions of the diffracted peaks alongside their intensity provide a specific information about the unite cell such as height, sheets diameter and inter-lamellar distance as well as aromaticity [48]. Basically, the XRD pattern of crude oil asphaltenes consists of four major bands. These bands are the γ-band, graphene (002), 10-band and 11-band, which are diffracted over 2θ region at around 20°, 25°, 40° and 80° respectively. Fig. 2 reveals the detected peaks position of KEC asphaltene sample. The first two bands (γ and 002) correspond to the distance between the saturated sidechains including the condensed saturated rings and distance between the stacked aromatic sheets respectively [12]. While, both 10 and 11 bands are scattered from the in-plane structure of aromatic core, which represent the average diameter and neighbours' aromatic layers [31]. It is known that the intensity of 11-band is often too weak and difficult to detect, thus the 10-band is commonly used to calculate the average aromatic sheet diameter [45]. (See Fig. 3.)

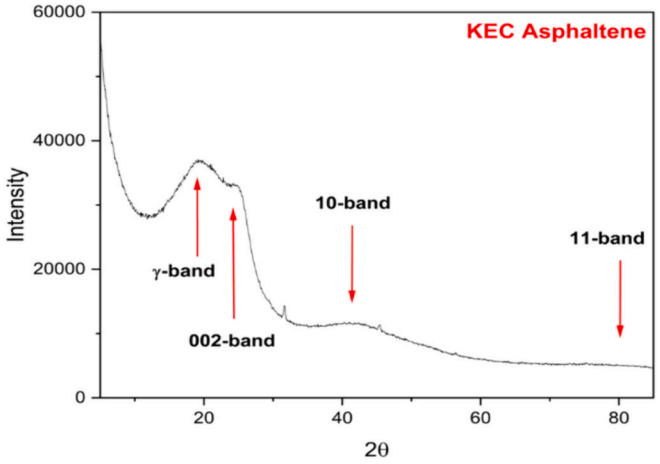

Fig. 2. X-ray diffraction pattern of KEC asphaltene.

Several studies have developed a set of theoretical equations prior to obtain the crystallite parameters and aromaticity, a more detailed explanation of the equation is described elsewhere [17,19,49–51]. Resolving the peaks of both γ-band and 002-band (graphene) derived from the XRD, allows calculating the area of each peak. Which subsequently can be used to determine the aromaticity from the structural unit of asphaltene using the equation as following:

$$f_a = C_A/(C_A + C_S) = C_A/C = A_{(002)}/(A_{(002)} + A_{(\gamma)}) \quad (1)$$

where C_A, $C_s$and C are the number of aromatic, saturated and total carbon atoms per structural unit respectively. It worthwhile to mention that f_a represent only the total aromatic carbon per stacked cluster that associated with 002-peak, which does not account for other aromatic carbon contribute to the γ-peak such as condensed naphthenic rings [48]. As a result, the value of f_a derived via XRD doesn't provide an accurate measurement of the true aromaticity value. Nonetheless, there are other techniques, such as NMR, can be utilised to determine the true aromaticity value of asphaltene molecular structure [10,48,52].

Based on the maximum of the graphene band, the Bragg relation is used to calculate the layer distance between the neighbouring aromatic sheets according to the following equation:

$$d_m = \lambda/(2sin\theta_{graphene-band}) \quad (2)$$

where λ is the wavelength of CuKα radiation and θ represents the Bragg's

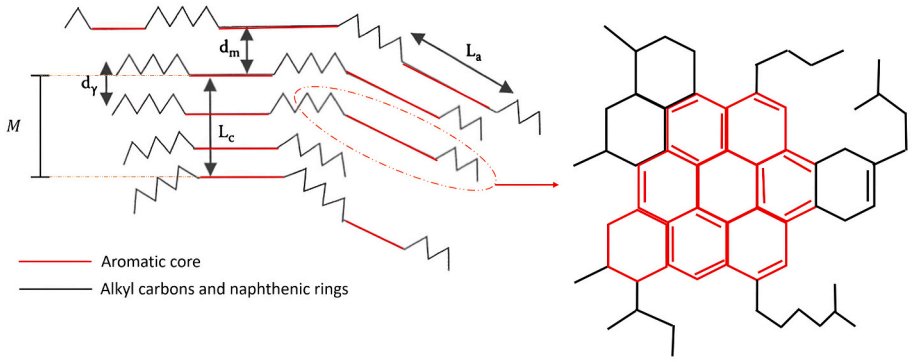

Fig. 3. Hypothetical illustration of the crystallite parameters dimensions in an asphaltene cluster (island model) [55,56].

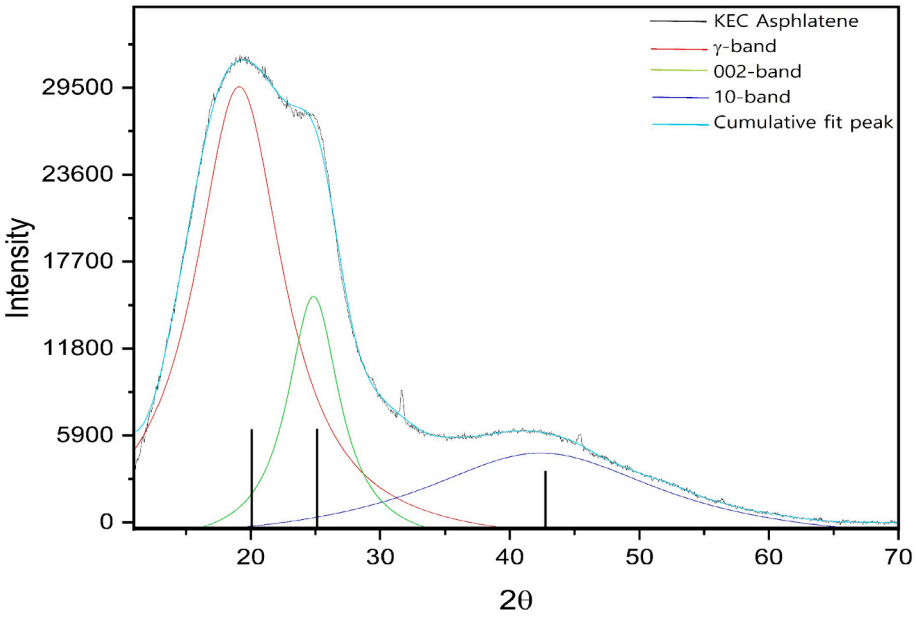

Fig. 4. XRD pattern of KEC asphaltene sample with curve fitting using Lorentzian distribution after adjusting the baseline.

angle of 002-band [53]. The distance between the saturated fragments (inter layer distance) including the aliphatic sidechains and saturated rings is measured from the γ-band according to:

$$d_\gamma = 5\,\lambda/\left(8sin\theta_{\gamma-band}\right) \tag{3}$$

where θ_γ is the Bragg's angle of γ-band [24]. The aromatic sheets average diameter is calculated from the following equation:

$$L_a = 1.84\lambda/(\omega\cos\theta_{10-band}) = 0.92/FWMH_{10-band} \tag{4}$$

where θ_{10} is the Bragg's angle of 10-band, while both $FWMH_{10-band}$ and ω represent the full width at half-maximum of the 10-band and band-width respectively [31]. The number of carbon atoms in the aromatic unit is calculated as following:

$$C_{au} = L_a + 1.23/0.65 \tag{5}$$

The average height of stacked aromatic sheets per cluster is given by the following relation:

$$L_c = 0.9\omega\cos\theta_{graphene-band} = 0.45/FWMH_{grapgene-band} \tag{6}$$

$FWMH_{grapgene-band}$ is the full width at half-maximum of the 002-band [19]. The number of stacked aromatic sheets per cluster is determined as follows:

$$M = (L_c/d_m) + 1 \tag{7}$$

The average number of aromatic rings per sheets is given as follows [54]:

$$NO_{ar} = L_a/2.667 \tag{8}$$

Lorentzian distribution is a profile fitting (de-convolution) model which involves a set of mathematical equations that are used to generate the expected shape of XRD profiles. This technique based on utilising the Levenberg-Marquardt nonlinear last-squares algorithm, which allows a better description of the profile parameters including peak position and intensity as well as line broadening [57]. As a result, the intensity, position, width, and FWHM as well as net areas of the peaks can be accurately measured. Fig. 4 reveals the de-convolution for the KEC asphaltene sample. Subsequently, the obtained parameters are substituted into eqs. (1–8) to determine the crystalline parameters of the sample. A detailed description of the profile fitting procedure for the X-ray patterns of petroleum asphaltene can be found elsewhere [45,53,58]. It worth mentioning that the baseline correction is essential for determining the sample independent parameters more accurately. As mentioned previously, both baseline and profile fitting were corrected and measured three times to attain high coefficient of determination ($R^2 \approx 0.99$) prior to ensure accuracy of the derived crystallite parameters.

Ball Milling Time	XRD Measurement	Lorentzian Function Profile
30 min	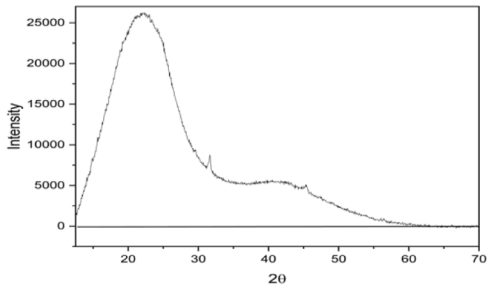	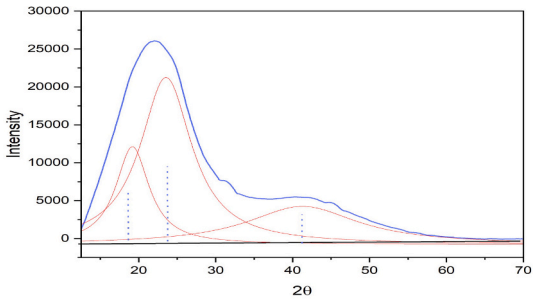
1 hr	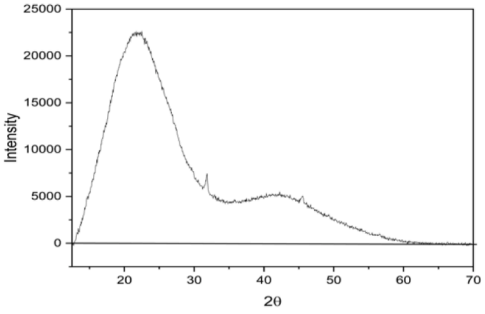	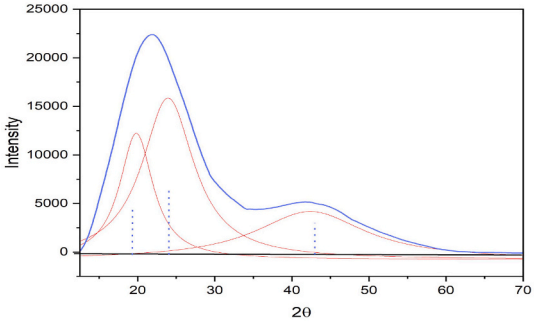
12 hr	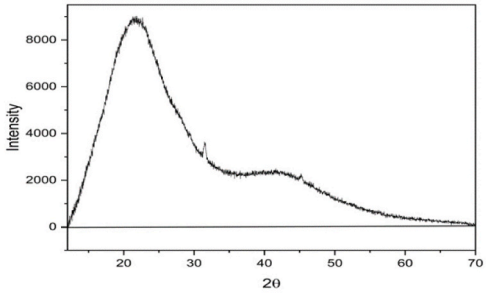	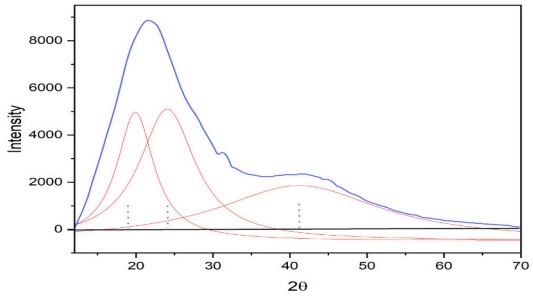
24 hr	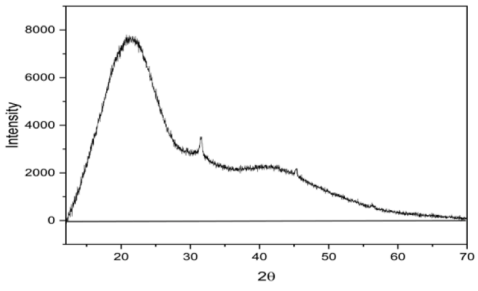	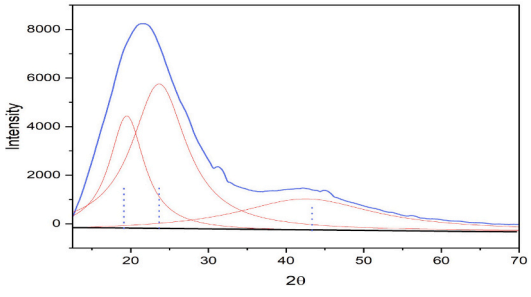

Fig. 5. XRD patterns of the ball milled KEC asphaltene samples with curve deconvolution using Lorentzian functions.

Table 2
Crystallite parameters derived from the XRD patterns of BM KEC asphaltene.

Ball milling	Crystallite parameters						
Time	d_m (Å)	d_y (Å)	L_a (Å)	L_c (Å)	M	NO_{ar}	C_{au}
0 h	3.6	5.5	16	24.6	8.0	6.8	27
30 min	3.9	5.7	20	9.7	3.5	7.4	32
1 h	3.9	5.8	20	9.6	3.5	7.5	33
3 h	3.9	5.8	14	10.0	3.5	5.0	23
6 h	4.0	5.8	18	10.0	3.6	7.0	30
12 h	3.9	5.7	13	9.2	3.3	6.4	23
24 h	3.9	5.7	16	9.3	3.2	6.5	26

3. Results and discussions

3.1. The influence of mechanical stress on crystal geometry

The X-ray measurement of the ball milled KEC asphaltene samples with their de-convoluted profiles using Lorentzian destitution are shown in Fig. 5. The determined structural parameters of the virgin KEC asphaltene sample (0 h) were compared to those calculated by AlHumaidan et al [33], whom studied the same asphaltene origin (KEC). The results were in a good agreement with their published data. After 30 min of BM, the value of aromatic sheet's layer distance (d_m) was increased from 3.6 Å to 3.9 Å. The value was further increased about 0.1 Å after 3 h. However, it remains constant at 3.9 Å throughout the BM experimentations. Although ball milling taking a place at ambient condition, the d_m value was considerably changed from 3.6 Å to 3.9 Å after 24 h of milling time.

Similarly, the distance between saturated sidechains (d_γ) was also influenced after using BM, with a 0.25 Å increment on average, see Table 2. Additionally, when compared to virgin asphaltene (Fig. 4), the scattered pattern of γ-band revealed considerable alterations as milling times increased. For instance, it was observed that the 1 h sample, and the subsequent BM samples, exhibited weak γ-band intensities, accompanied with a slight shifting in the band position as shown in Fig. 5. The results indicates that the applied mechanical stress induced crystal defects in the structural compounds related to the γ-band, leading to changes in their molecular geometry.

The average of the aromatic sheets' diameter (L_a) raised to 20 Å for the 30 min sample, while both 1 h and 6 h samples have nearly the same influence of the 30 min sample. However, the L_a value decreased to 14 Å and 13 Å for the 3 h and 12 h samples respectively, while the 24 h sample matched the original value (0 h). Which suggested that short milling period is more selective toward increasing the in-plane structural property, which tends to decrease with longer milling times (e.g. from 6 h of ball milling and above). In addition, it was observed that the number of carbon atoms in the aromatic unit (C_{au}) almost follows the same behaviour as the L_a parameter

A significant reduction in the height of stacked aromatic perpendicular to the sheets plane (L_c) was observed after 30 min of milling times, the L_c value was decreased to 9.7 Å, corresponding to a 61% reduction. The number almost remains constant from 1 h till 6 h with average L_c value of 9.7 Å, but begins to slightly decrease to 9.3 Å with higher milling times. On the other hand, the number of stacked aromatic sheets per cluster (M) also showed a major reduction that is proportional to L_c value. Where the M value was decreased to 3.5 for the 30 min sample, then became 3.5 and remained unchanged as the milling time further increases up to 6 h. However, the value was decreased to 3.2 for the 24 h sample. These results indicated that short ball milling prompts a scission of the aromatic core, splitting it into two or three nanoclusters with average of ≈ 3 stacked aromatic sheets per cluster, while longer milling times do not have much effect. It is therefore suggested the mechanical interaction of ball-powder-ball would play a major role in re-defining the core dimension of the aromatic structure at molecular level regardless of the input heat.

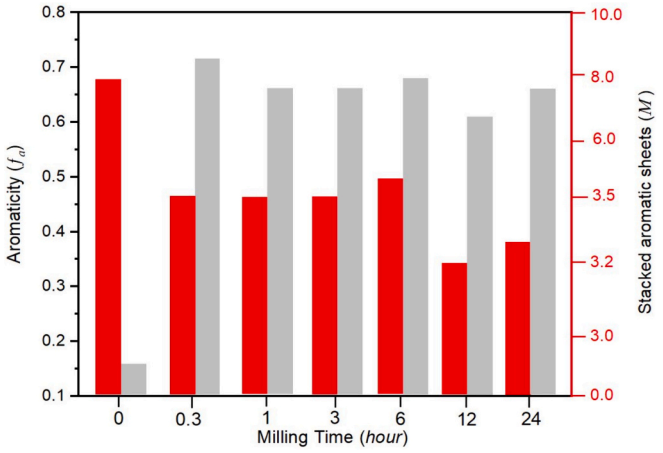

Fig. 6. Aromaticity of KEC asphaltene as function of up to 24 h of BM.

Additionally, the number of aromatic rings per sheets (NO_{ar}) wasn't drastically affected during the BM experimentations. It was noticed that the average number of NO_{ar} is 6.7 and 6.4, respectively at low and high milling time. It is worth noting that mechanical inducement using ball milling technique has shown the ability of modifying the molecular structure of the KEC asphaltene, without requiring of a heating source.

3.2. Asphaltene crystallinity

A change in asphaltene crystallinity after being exposed to BM was also assessed using XRD. As seen in Fig. 5, the background noise level (baseline) is getting greater as BM times increase, indicating of producing more disorganised arrangement of asphaltene molecules in form of amorphous phase [44]. Further, both of 002-peak and 10-peak were shifted after 24-h of BM, which were identified at around 23.9° and 43.7° respectively (see Fig. 5, 24-h sample). The peaks shift was attributed to the alteration among the lattice parameters in asphaltene crystal, indicating of phase transition into amorphous carbon of different ranged order [39].

Similarly, the Interlayer spacing between the neighbouring aromatic sheets (d_m) was increased about 0.35 Å after BM (Table 2). Although, thermal expansion increases the layer distance which would lead to increase the active site for foreign heteroatoms [59] (i.e., intercalation), the average d_m value of various thermally treated asphaltenes is 3.5 Å roughly [31], whereas the determined value after BM experimentation is 3.9 Å. Therefore, it is suggested that the mechanical stress induced lattice imperfection, resulting in disturbing the atomic arrangement of the aromatics layer [60]. To elaborate the influence of d_m value in the crystallinity of asphaltene, the Interlayer spacing of pure graphite ranging from 3.36 to 3.37 Å [61], which is lower than those values of the ball milled samples 3.9–4.0 Å. Thus, it is clearly evident that asphaltene crystallinity has decreased significantly.

Although, the proposed aromaticity equation (1) doesn't represent the true aromaticity value of asphaltene, the great increment in the f_a value (Fig. 6) suggested that the milled sample experienced several chemical transformations: dissociation and fragmentation followed by cyclisation and polymerisation (aromatisation), as well as a physical separation of the stacked aromatic sheets per cluster caused by the clusters splitting. As seen from Fig. 6, the change in the aromaticity value is linked with a substantial change in the M value. However, describing the crystal breaking and alignment mechanism based on analysing the aromaticity value is limited. Therefore, the transformation mechanism will be explained in the following section.

Other study found that asphaltene contain a considerable proportion

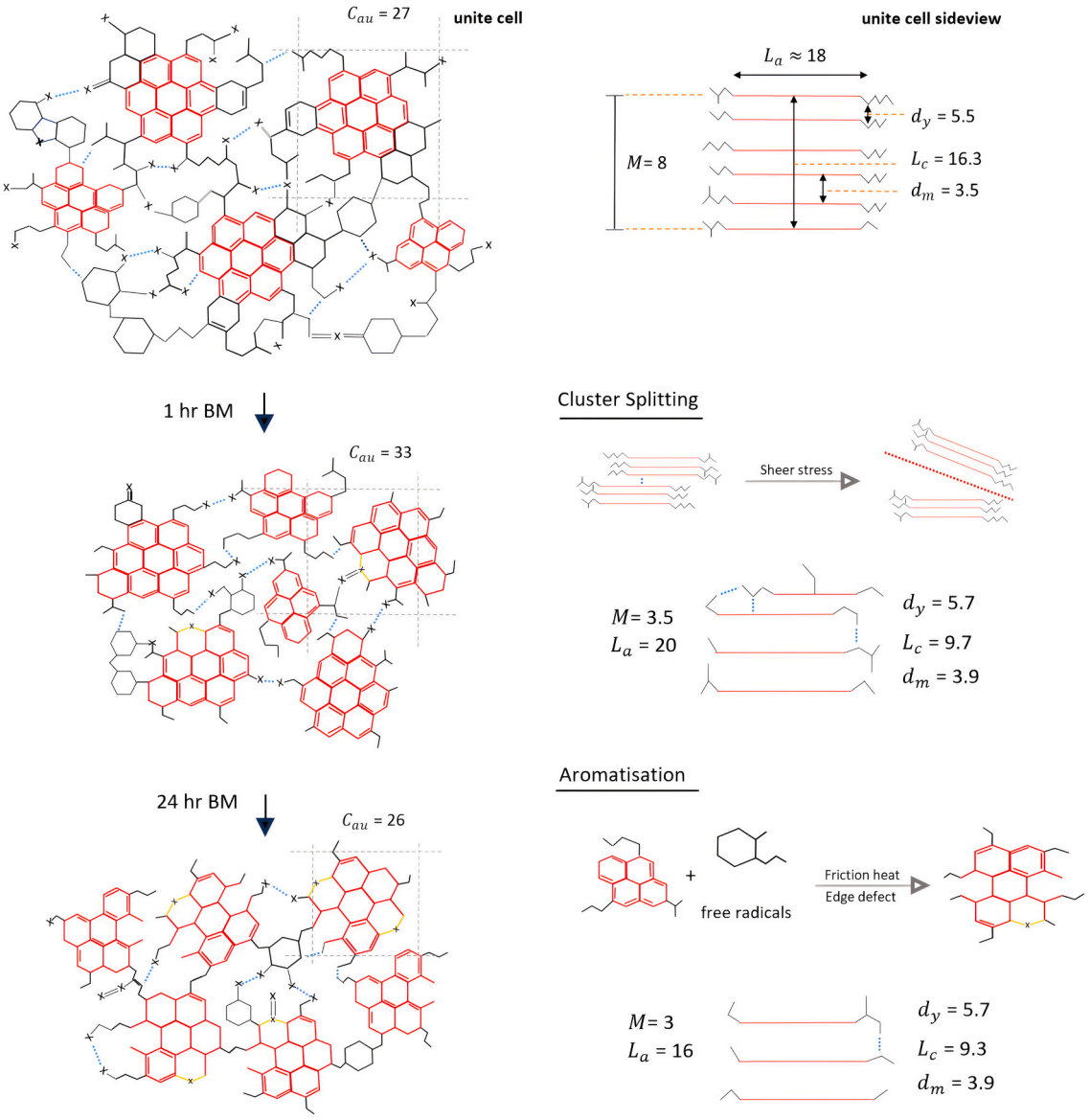

Fig. 7. Hypothetical Illustration of asphaltene crystal breaking and alignment during BM.

of ordered materials in form of amorphous carbons, that start getting changed in the temperature ranges of 70 to 170 °C [62]. Therefore, the energy generated from the continuous balls collisions (i.e., sheer force) during longer milling period can promote a phase change in the crystal structure of asphaltene. Subsequently, resulting in generating or increasing the proportion of highly disordered materials of short or medium range order [44].

3.3. Transformations mechanism during Ball milling

Several changes were observed in asphaltene's molecular structure during different stages (periods) of BM. Two mechanisms were proposed: physical scissoring and chemical transforming, which are illustrated accordingly in Fig. 7. In the former, a clusters separation can be observed at earlier stages of the BM experimentation, in particular 30 min and 1-h samples. As seen in Table 2, the number of carbon atoms in the aromatic unit (C_{au}) increased despite the reduction of the aromatic sheets number per cluster (M). This suggested an interaction between the unpaired surface (fresh active site) of the aromatics layer with the neighbouring aliphatic chains, leading to a considerable increase in the average carbon atoms within the unit cell. Also, the rapid (abnormal) rise in the graphene-peak' intensity after 30 min of BM can only be attributed to the massive accumulation of aromatic carbons of 3.5 sheets caused by cluster splitting, which disturbing the arrangement of the peripheral carbons as indicated from the XRD profile of γ-band after earlier stages of BM.

In the latter, the transition of aliphatic side chains into aromatic carbons and vice versa can be observed by tracking the associated XRD profile parameters of γ-band. The continuous alternating of γ-band during BM experiments indicates that the chemical transformation is heterogeneous. For instance, both the intensity and area under curve started increasing gradually as seen from XRD profile (Fig. 5) of sample 30 min to 12 h, corresponding to a considerable change in the M and C_{au} values from 3.5 and 32 to 3.3 and 23 respectively. It is suggested that the carbon rings that less stably attached to the aromatic layer edge experienced an edge fictionalisation that leads to open the aromatic ring, which can be evident from the reduction in the f_a value from 73.4 to 63.6, see Fig. 6. It was reported that BM mechanically breaks C—C bonds within graphite layers, producing unsaturated graphene flakes with highly reactive edges [63].

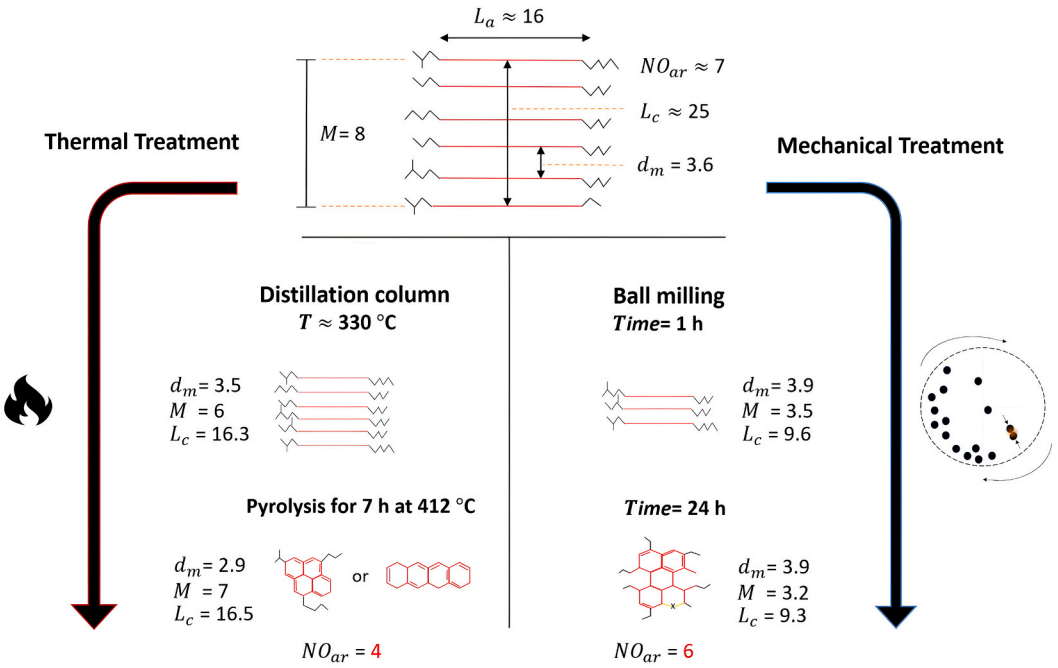

Fig. 8. Illustrates the molecular revolution of KEC asphaltene sample under mechanical and heat stress [32].

However, the reduction in the γ-band intensity as BM severity increase at later stages of (24 h sample) suggested a formation of cyclic fragments of more stable phase, mainly graphene basal plane, by combining the loosened carbon rings and the aliphatic chains. The chemical transformation (aromatisation) during BM was also observed in other studies. It was found the aromatic content of oily sludge increased from 30.0 to 38.0% after longer BM times [40]. According to Timko and his group, the amount of side chains fragments decreases with increase in graphitization during ball milling of hydrothermal char. It was found that the loosened aliphatic bonds form a site bearing the free radicals, then recombine to form aromatic ring [64].

It's important to mention that the average number of the aromatic sheets remains almost constant (≈3) throughout the BM experimentation. According to this, the interaction of π–π core stacking might only account for three sheets per cluster, which was weakly coupled to other sheets of the same number. However, there has been much debate about the nature of the out-of-plane π–π core interactions [65].

3.4. Mechanical stress vs. heat stress

In light of the information obtained in Table 2, it appears that the impact of BM on the crystallite parameters is significantly different than that of heat treatment. For instance, Asaoka et al. studied the influence of catalytic hydrocracking in the crystal parameters of the feed and product for three various asphaltenes samples over 350 to 430 °C temperature range. It was found that the average values of L_c and M for Boscan crude, Athabasca bitumen and Khafji vacuum residue were around 19 Å and 6, respectively [20]. AlHumaidan et al [33], investigated the structural paraments of KEC asphaltene under several carbonisation temperature up to 950 °C. Their study shows that at 600 to 950 °C, the average L_c and M values are 17.7 Å and 6, respectively.

To illustrate the impact of mechanical and heat stress on crystallite parameters, the molecular revolutions of KEC asphaltene sample under mechanical and heat stress are summarised in Fig. 8. As the diagram shows, the aid of heat has not considerably altered the L_c value nor the M value, whereas these parameters were substantially reduced after using BM. Additionally, Ali et al [66], also investigated the crystallite parameters of two asphaltene samples obtained from Kuwaiti oil. The determined L_c and M values for the AR -asphaltene were 16.6 Å and 6, while the VR-asphlatene were and 14.6 Å and 5, respectively. As a result, it can be observed that both L_c and M parameters are more sensitive to mechanical stress in comparation to heat stress. For better evaluation between the impact of mechanical stress against heat stress, an overview of the stacked aromatic sheets per cluster of different asphaltene origins over a wide range of thermodynamic states is summarised in Table 3.

Table 3
Aromatic sheets number per cluster originating from various origin of asphaltenes.

Asphaltene origin	Process conditions		*M*		Ref
	Temperature	Time	Before	After	
Boscan crude			6.5	6.6	
Athabasca bitumen	360–430 °C	0.2–1.5 h	5.7	6.0	[20]
Khafji VR			6.4	6.9	
Gudao VR	165 °C	5.0 h	5.8	5.2	
Shanjiasi VR			5.4	5.2	[25]
Maya VR					
Khafji VR	30–300 °C	–	~8.0	~5.6	[67]
Iranian light VR					
Kuwaiti VR	430 °C	–	5.0	5.0	[27]
KEC AR			6.0	7.0	
KHC AR	412 °C	7.0 h	5.0	7.0	[32]
EOC AR			7.0	6.0	
Hyundai oil VR					
Hydrothermal cracking	380–430 °C	1.0–20.0 h	5.1	~5.6	[68]
Catalytic Hydrothermal cracking			5.1	~5.5	
Hydrotreated AR	350 °C	5.0 h	6.9	5.5	
Hydrotreated blend AR + LCO			6.9	4.9	[54]
Ratawi Burgan VR			5.0	~4.5	
Lower Fars VR	415–430 °C	0.5–1.0 h	5.0	~4.0	[48]
Eocene VR			5.0	~4.0	

4. Conclusion

This work demonstrated the influence of a mechanical BM on the crystallite paraments of KEC asphaltene. XRD was utilised to study the

molecular structure behaviour over various milling times. The computed parameters indicate that the height of stacked aromatic sheets per cluster (L_c) was significantly reduced due to physical scission of the cluster. In turn, increases the content of aromatic carbons of 3 sheets per cluster (M). Moreover, as milling time increase, the γ-band is getting weak, owing to phase changes in the associated crystal structures. It is suggested that a number of the dissociated aliphatic bonds would form a site bearing the free radicals, some of which recombine to form condensated rings whilst those loosened aliphatic chains re-distribute far from each other as evident by the considerable change in d_γ value. This implies that the mechanical excitation will move saturated compounds closer to aromatic basal planes as sidechains or bridges (linkers). A high background intensity was observed in XRD profiles of 12 and 24 h samples. This is an indication of generating or increasing the proportion of highly disordered materials of short or medium range order. Although the aromaticity (f_a) equation doesn't represent the true aromaticity value, the significant increment in the value reveals that mechanical stress induces polymerisation and aromatisation. In addition, the results showed the core structural parameters (e.g., L_c and M) are more sensitive to mechanical stress over heat stress.

CRediT authorship contribution statement

Fahad Al-Ajmi: Writing – original draft, Validation, Resources, Methodology, Formal analysis, Conceptualization. **Jun Li:** Writing – review & editing, Supervision, Resources, Methodology.

Declaration of Competing Interest

Fahad Alajmi reports financial support was provided by Kuwait Institute for Scientific Research. If there are other authors, they declare that they have no known competing financial interests or personal relationships that could have appeared to influence the work reported in this paper.

Data availability

No data was used for the research described in the article.

Acknowledgments

The authors gratefully thank the Kuwait Institute for Scientific Research for their financial support to Fahad Alajmi. Also, the authors would like to thank Dr. Faisal AlHumaidan for his support throughout this research.

References

[1] T. Jiang, X. He, B. Su, P.H. Havea, K. Wei, Z.W. Kundzewicz, et al., COP 28: challenge of coping with climate crisis, Innovation 5 (1) (2024).
[2] Y. Dong, Q. Zhao, Y. Zhou, L. Zheng, H. Jin, B. Bawaa, et al., Kinetic study of asphaltenes phase separation in supercritical water upgrading of heavy oil, Fuel Process. Technol. 241 (2023 Mar 1).
[3] S. Ali, P.M. Ismail, M. Humayun, M. Bououdina, L. Qiao, Tailoring 2D metal-organic frameworks for enhanced CO2 reduction efficiency through modulating conjugated ligands, Fuel Proces Technol [Internet] 255 (2024 May 1) 108049 [cited 2024 Feb 8]. Available from, https://linkinghub.elsevier.com/retrieve/pii/S0378382024000195.
[4] E.Y. Kovalenko, N.N. Gerasimova, T.A. Sagachenko, R.S. Min, Y.F. Patrakov, Characteristics of products of thermal decomposition of heavy oil asphaltenes under supercritical conditions, Energy Fuels. 34 (8) (2020 Aug 20) 9563–9572.
[5] F.S. Alhumaidan, A. Hauser, M.S. Rana, H.M.S. Lababidi, Impact of thermal treatment on asphaltene functional groups, Energy Fuels 30 (4) (2016 Apr 21) 2892–2903.
[6] L. Yuan, Y. Zhang, S. Liu, Y. Zhang, Y. Song, Investigation of the effect of CO2 on asphaltene deposition and flow mechanism under nano-confined environment, J. Mol. Liq. 396 (2024 Feb 15).
[7] J.J. Li, Gz Deng, Xd Tang, Jw Wang, C. Yang, Sh. Ling, The effect of chlorella hydrothermal products on the heavy oil upgrading process, Fuel Process. Technol. 241 (2023 Mar 1).
[8] T.V. Cheshkova, V.P. Sergun, E.Y. Kovalenko, N.N. Gerasimova, T.A. Sagachenko, R.S. Min, Resins and asphaltenes of light and heavy oils: their composition and structure, Energy Fuels. 33 (9) (2019 Sep 19) 7971–7982.
[9] A. Hauser, F. Alhumaidan, H. Al-Rabiah, NMR investigations on products from thermal decomposition of Kuwaiti vacuum residues, Fuel 113 (2013 Nov 1) 506–515.
[10] H.M.S. Lababidi, H.M. Sabti, F.S. Alhumaidan, Changes in asphaltenes during thermal cracking of residual oils, Fuel 117 (PART A) (2014 Jan 30) 59–67.
[11] J.G. Speight, R.B. Long, The concept of asphaltenes revisited, Fuel Sci. Technol. Int. [Internet]. 14 (1–2) (1996 Jan 1) 1–12. Available from: https://doi.org/10.1080/08843759608947559.
[12] O.C. Mullins, H. Sabbah, J. Eyssautier, A.E. Pomerantz, L. Barré, A.B. Andrews, et al., Advances in asphaltene science and the Yen–Mullins model, Energy Fuels [Internet]. 26 (7) (2012 Jul 19) 3986–4003. Available from: https://doi.org/10.1021/ef300185p.
[13] A.M. Aitani, Oil refining and products, Encycl. Energy (2004 Jan 4) 715–729.
[14] A. Demirbas, O. Taylan, Removing of resins from crude oils, Pet. Sci. Technol. [Internet] 34 (8) (2016 Apr 17) 771–777. Available from, https://doi.org/10.1080/10916466.2016.1163397.
[15] Y. Bouhadda, D. Bormann, E. Sheu, D. Bendedouch, A. Krallafa, M. Daaou, Characterization of Algerian Hassi-Messaoud asphaltene structure using Raman spectrometry and X-ray diffraction, Fuel 86 (12–13) (2007 Aug 1) 1855–1864.
[16] A.M. McKenna, A.G. Marshall, R.P. Rodgers, Heavy petroleum composition. 4. Asphaltene compositional space, Energy Fuels [Internet]. 27 (3) (2013 Mar 21) 1257–1267. Available from: https://doi.org/10.1021/ef301747d.
[17] J. Christopher, A.S. Sarpal, G.S. Kapur, A. Krishna, B.R. Tyagi, M.C. Jain, et al., Chemical structure of bitumen-derived asphaltenes by nuclear magnetic resonance spectroscopy and X-ray diffractometry, Fuel 75 (8) (1996 Jun 1) 999–1008.
[18] G. Mushrush, Petroleum Products: Instability and Incompatibility, CRC Press, 2014 Jul 22.
[19] T.F. Yen, J.G. Erdman, S.S. Pollack, Investigation of structure of petroleum asphaltenes by X-ray diffraction, Anal. Chem. 33 (11) (1961) 1587.
[20] S. Asaoka, S. Nakata, Y. Shiroto, C. Takeuchi, Asphaltene cracking in catalytic hydrotreating of heavy oils. 2. Study of changes in asphaltene structure during catalytic hydroprocessing, Indust. Eng. Chem. Process Design Dev. 22 (2) (1983) 242–248.
[21] M. Yasar, S. Akmaz, M.A. Gurkaynak, Investigation of the molecular structure of Turkish asphaltenes, Pet. Sci. Technol. [Internet]. 27 (10) (2009 Aug 19) 1044–1061. Available from: https://doi.org/10.1080/10916460802455913.
[22] Y. Yi, S. Li, F. Ding, H. Yu, Change of asphaltene and resin properties after catalytic aquathermolysis, Pet. Sci. [Internet]. 6 (2) (2009) 194–200. Available from: https://doi.org/10.1007/s12182-009-0031-y.
[23] J.C. Poveda-Jaramillo, D.R. Molina-Velasco, N.A. Bohorques-Toledo, M.H. Torres, E. Ariza-León, Chemical characterization of the asphaltenes from Colombian Colorodo light crude oil, CT&F-Ciencia Tecnologia Y Futuro. 6 (3) (2016) 105–122.
[24] H. Díaz-Sánchez, J.B. Rojas-Trigos, C. Leyva, F. Trejo-Zárraga, An approach for determination of asphaltene crystallite by X-ray diffraction analysis: a case of study, Pet. Sci. Technol. [Internet]. 35 (13) (2017 Jul 3) 1415–1420. Available from: https://doi.org/10.1080/10916466.2017.1336771.
[25] Y. Zhang, C. Liu, W. Liang, Study of asphaltenes in two Chinese asphalts by X-ray diffraction, Fuel Sci. Technol. Int. [Internet]. 7 (7) (1989 Jan 1) 919–929. Available from: https://doi.org/10.1080/08843758908962274.
[26] S.K. Maity, S. Kumar, M. Srivastava, A.S. Kharola, K.K. Maurya, S. Konathala, et al., Characterization of asphaltenic material obtained by treating of vacuum residue with different reactive molecules, Fuel 149 (2015 Jun 1) 8–14.
[27] G. Michael, M. Al-Siri, Z.H. Khan, F.A. Ali, Differences in average chemical structures of asphaltene fractions separated from feed and product oils of a mild thermal processing reaction, Energy Fuels [Internet]. 19 (4) (2005 Jul 1) 1598–1605. Available from: https://doi.org/10.1021/ef049854l.
[28] T.V. Cheshkova, A.A. Grinko, R.S. Min, T.A. Sagachenko, Structural transformations of heavy oil asphaltenes in the course of heat treatment, Petrol. Chem. [Internet]. 62 (2) (2022) 214–221. Available from: https://doi.org/10.1134/S0965544122060093.
[29] R. Tanaka, J.E. Hunt, R.E. Winans, P. Thiyagarajan, S. Sato, T. Takanohashi, Aggregates structure analysis of petroleum asphaltenes with small-angle neutron scattering, Energy Fuels [Internet]. 17 (1) (2003 Jan 1) 127–134. Available from: https://doi.org/10.1021/ef020019i.
[30] T. Takatsuka, S.I. Inoue, Y. Hori, Role of asphaltenes cracking in bottoms conversion, Pet. Technol. Q. 61–8 (1999).
[31] Z. Sadeghtabaghi, A.R. Rabbani, A. Hemmati-Sarapardeh, A review on asphaltenes characterization by X-ray diffraction: fundamentals, challenges, and tips, J. Mol. Struct. 1238 (2021 Aug 15) 130425.
[32] A. Hauser, D. Bahzad, A. Stanislaus, M. Behbahani, Thermogravimetric analysis studies on the thermal stability of asphaltenes: pyrolysis behavior of heavy oil asphaltenes, Energy Fuels [Internet]. 22 (1) (2008 Jan 1) 449–454. Available from: https://doi.org/10.1021/ef700477a.
[33] F.S. AlHumaidan, M.S. Rana, M. Vinoba, H.M. AlSheeha, A.A. Ali, R. Navvamani, Synthesis of graphene derivatives from asphaltenes and effect of carbonization temperature on their structural parameters, RSC Adv. 13 (12) (2023) 7766–7779.
[34] M.H. Enayati, F.A. Mohamed, Application of mechanical alloying/milling for synthesis of nanocrystalline and amorphous materials, Int. Mater. Rev. [Internet]. 59 (7) (2014 Sep 1) 394–416. Available from: https://doi.org/10.1179/1743280414Y.0000000036.
[35] M.S. El-Eskandarany, S.M. Al-Salem, N. Ali, M. Banyan, F. Al-Ajmi, A. Al-Duweesh, From gangue to the fuel-cells application, Sci. Rep. [Internet]. 10 (1) (2020) 20022. Available from: https://doi.org/10.1038/s41598-020-76503-6.

[36] M.S. El-Eskandarany, M. Banyan, F. Al-Ajmi, Discovering a new MgH_2 metastable phase, RSC Adv. 8 (56) (2018) 32003–32008.
[37] H. Almatrouk, F. Al-Ajmi, D. Son, V. Chihaia, V. Alexiev, The Pressure-Temperature Phase Diagram Assessment for Magnesium Hydride Formation/Decomposition Based on DFT and CALPHAD Calculations 4, 2021 Apr 20, p. 467.
[38] M.S. El-Eskandarany, N. Ali, F. Al-Ajmi, M. Banyan, Phase transformations from nanocrystalline to amorphous $(Zr_{70}Ni_{25}Al_5)_{100-x}W_x$ (x; 0, 2, 10, 20, 35 at. %) and subsequent consolidation, Nanomaterials 11 (11) (2021).
[39] M.S. El-Eskandarany, A. Al-Hazza, L.A. Al-Hajji, N. Ali, A.A. Al-Duweesh, M. Banyan, et al., Mechanical milling: a superior nanotechnological tool for fabrication of nanocrystalline and nanocomposite materials, Nanomaterials [Internet]. 11 (10) (2021). Available from: https://www.mdpi.com/2079-4991/11/10/2484.
[40] H.S. Chen, Q.M. Zhang, Z.J. Yang, Y.S. Liu, Research on treatment of oily sludge from the tank bottom by ball milling combined with ozone-catalyzed oxidation, ACS Omega [Internet]. 5 (21) (2020 Jun 2) 12259–12269. Available from: https://doi.org/10.1021/acsomega.0c00958.
[41] N.J. Welham, P.G. Chapman, Mechanical activation of coal, Fuel Process. Technol. 68 (1) (2000) 75–82.
[42] A.M.A. Ahmed, Preparation of N-Doped Porous Catalyst derived from Petroleum Coke using Ball Milling for the Oxidative Desulfurization of Fuel, 2022.
[43] V. Kurian, Asphaltene Gasification: Soot Formation and Metal Distribution, 2016.
[44] O.O. Sonibare, T. Haeger, S.F. Foley, Structural characterization of Nigerian coals by X-ray diffraction, Raman and FTIR spectroscopy, Energy 35 (12) (2010 Dec 1) 5347–5353.
[45] M.N. Siddiqui, M.F. Ali, J. Shirokoff, Use of X-ray diffraction in assessing the aging pattern of asphalt fractions, Fuel 81 (1) (2002 Jan 1) 51–58.
[46] F.S. AlHumaidan, M.S. Rana, Determination of asphaltene structural parameters by Raman spectroscopy, J. Raman Spectrosc. [Internet]. 52 (11) (2021 Nov 1) 1878–1891. Available from: https://doi.org/10.1002/jrs.6233.
[47] R.R. Coelho, I. Hovell, M.B. De Mello Monte, A. Middea, A.L. De Souza, Characterisation of aliphatic chains in vacuum residues (VRs) of asphaltenes and resins using molecular modelling and FTIR techniques, Fuel Process. Technol. 87 (4) (2006 Apr 1) 325–333.
[48] F.S. Alhumaidan, A. Hauser, M.S. Rana, H.M.S. Lababidi, M. Behbehani, Changes in asphaltene structure during thermal cracking of residual oils: XRD study, Fuel 150 (2015 Jun 15) 558–564.
[49] J.W. Shirokoff, M.N. Siddiqui, M.F. Ali, Characterization of the structure of Saudi crude asphaltenes by X-ray diffraction, Energy Fuels [Internet]. 11 (3) (1997 May 1) 561–565. Available from: https://doi.org/10.1021/ef960025c.
[50] C.S. Wen, G.V. Chilingarian, T. Fu Yen, Chapter 7 Properties and Structure of Bitumens. Developments in Petroleum Science 7(C), 1978 Jan 1, pp. 155–190.
[51] M.A. Sadeghi, G.V. Chilingarian, T.F. Yen, X-ray-diffraction of asphaltenes, Energy Sources 8 (2–3) (1986) 99–123.
[52] F.S. AlHumaidan, A. Hauser, M.S. Rana, H.M.S. Lababidi, NMR characterization of asphaltene derived from residual oils and their thermal decomposition, Energy Fuels [Internet]. 31 (4) (2017 Apr 20) 3812–3820. Available from: https://doi.org/10.1021/acs.energyfuels.6b03433.
[53] T.F. Yen, Chapter 5 Multiple structural orders of asphaltenes, in: Developments in Petroleum Science 40(PA), 1994 Jan 1, pp. 111–123.
[54] Y.J. Liu, Z.F. Li, Structural characterisation of asphaltenes during residue hydrotreatment with light cycle oil as an additive, J. Chem. [Internet] 2015 (1) (2015 Jan 1) 580950. Available from, https://doi.org/10.1155/2015/580950.
[55] J. Ancheyta, F. Trejo, M.S. Rana, Asphaltenes: Chemical Transformation during Hydroprocessing of Heavy Oils [Internet], CRC Press, 2010 (Chemical Industries). Available from: https://books.google.co.uk/books?id=uP_LBQAAQBAJ.
[56] O.C. Mullins, The asphaltenes, in: R.G. Cooks, E.S. Yeung (Eds.), Annual Review of Analytical Chemistry Vol 4, 2011, pp. 393–418.
[57] R. Jenkins, W.N. Schreiner, Profile Fitting for quantitative analysis in X-ray powder diffraction, Advances in X-ray Analysis [Internet]. 1982;26 (2019/03/06) 141–147. Available from: https://www.cambridge.org/core/product/D6C4ED8C45A1BA8B6AC98E058E673D72.
[58] I. Schwager, P.A. Farmanian, J.T. Kwan, V.A. Weinberg, T.F. Yen, Characterization of the microstructure and macrostructure of coal-derived asphaltenes by nuclear magnetic-resonance spectrometry and X-ray-diffraction, Anal. Chem. 55 (1) (1983) 42–45.
[59] O.E. Medina, J. Gallego, N.N. Nassar, S.A. Acevedo, F.B. Cortés, C.A. Franco, Thermo-oxidative decomposition behaviors of different sources of n-C7 Asphaltenes under high-pressure conditions, Energy Fuel 34 (7) (2020) 8740–8758.
[60] A. Guinier, X-ray Diffraction in Crystals. Imperfect Crystals, and Amorphous Bodies Dorer, 1963.
[61] R.S. Aga, C.L. Fu, M. Krčmar, J.R. Morris, Theoretical investigation of the effect of graphite interlayer spacing on hydrogen absorption, Phys. Rev. B Condensed Matter Mater. Phys. 76 (16) (2007) 165404.
[62] Y.M. Ganeeva, T.N. Yusupova, G.V. Romanov, N.Y. Bashkirtseva, Phase composition of asphaltenes, J. Therm. Anal. Calorim. [Internet]. 115 (2) (2014) 1593–1600. Available from: https://doi.org/10.1007/s10973-013-3442-3.
[63] A. Bellunato, H. Arjmandi Tash, Y. Cesa, G.F. Schneider, Chemistry at the edge of graphene, ChemPhysChem [Internet]. 17 (6) (2016 Mar 16) 785–801. Available from: https://doi.org/10.1002/cphc.201500926.
[64] M.T. Timko, A.R. Maag, J.M. Venegas, B. McKeogh, Z.Y. Yang, G.A. Tompsett, et al., Spectroscopic tracking of mechanochemical reactivity and modification of a hydrothermal char, RSC Adv. 6 (15) (2016) 12021–12031.
[65] K. Carter-Fenk, J.M. Herbert, Reinterpreting π-stacking, Phys. Chem. Chem. Phys. 22 (43) (2020) 24870–24886.
[66] F.A. Ali, N. Ghaloum, A. Hauser, Structure representation of asphaltene GPC fractions derived from Kuwaiti residual oils, Energy Fuels [Internet]. 20 (1) (2006 Jan 1) 231–238. Available from: https://doi.org/10.1021/ef050130z.
[67] R. Tanaka, E. Sato, J.E. Hunt, R.E. Winans, S. Sato, T. Takanohashi, Characterization of asphaltene aggregates using X-ray diffraction and small-angle X-ray scattering, Energy Fuels [Internet]. 18 (4) (2004 Jul 1) 1118–1125. Available from: https://doi.org/10.1021/ef034082z.
[68] N.T. Nguyen, K.H. Kang, C.W. Lee, G.T. Kim, S. Park, Y.K. Park, Structure comparison of asphaltene aggregates from hydrothermal and catalytic hydrothermal cracking of C5-isolated asphaltene, Fuel [Internet]. 235 (2019) 677–686. Available from, https://www.sciencedirect.com/science/article/pii/S0016236118313942.